A comparative study revealed hyperspectral imaging as a potential standardized tool for the analysis of cuticle tanning over insect development

Virginie Lacotte, Elisa Dell'aglio, Sergio Peignier, Fadéla Benzaoui, Abdelaziz Heddi, Rita Rebollo, Pedro da Silva

Heliyon 9 (2023) e13962

Contents lists available at ScienceDirect

Heliyon

journal homepage: www.cell.com/heliyon

Research article

A comparative study revealed hyperspectral imaging as a potential standardized tool for the analysis of cuticle tanning over insect development

Virginie Lacotte [*,1], Elisa Dell'Aglio [1], Sergio Peignier, Fadéla Benzaoui, Abdelaziz Heddi, Rita Rebollo, Pedro Da Silva [**]

Univ Lyon, INSA Lyon, INRAE, BF2I, UMR 203, 69621 Villeurbanne, France

A B S T R A C T

Cereal-feeding beetles are a major risk for cereal crop maintenance. Cereal weevils such as *Sitophilus oryzae* have symbiotic intracellular bacteria that provide essential aromatic amino acid to the host for the biosynthesis of their cuticle building blocks. Their cuticle is an important protective barrier against biotic and abiotic stresses, providing high resistance from insecticides. Quantitative optical methods specialized in insect cuticle analysis exist, but their scope of use and the repeatability of the results remain limited. Here, we investigated the potential of Hyperspectral Imaging (HSI) as a standardized cuticle analysis tool. Based on HSI, we acquired time series of average reflectance profiles from 400 to 1000 nm from symbiotic (with bacteria) and aposymbiotic (without bacteria) cereal weevils *S. oryzae* exposed to different nutritional stresses. We assessed the phenotypic changes of weevils under different diets throughout their development and demonstrated the agreement of the results between the HSI method and the classically used Red-Green-Blue analysis. Then, we compared the use of both technologies in laboratory conditions and highlighted the assets of HSI to develop a simple, automated, and standardized analysis tool. This is the first study showing the reliability and feasibility of HSI for a standardized analysis of insect cuticle changes.

1. Introduction

Cereal-feeding beetles are among the most dangerous risks for cereal agriculture, as they are responsible for 40% of storage grain loss [1]. Several species of the genus *Sitophilus*, including *Sitophilus oryzae*, *Sitophilus zeamais* and *Sitophilus granarius* are among the most destructive pests widespread in America, Asia, Africa, and Europe. Such weevil infestations in tropical and subtropical regions are commonly responsible for 12 to 20% of grain loss [2]. The wide distribution of these insects across the globe together with the emergence of resistance against the most common insecticide treatment (phosphine) have increased the interest on weevils' biology and ecology [3,4].

An important protective structure of cereal-feeding weevils and beetles is their external cuticle, which is chitin based and comprises proteins and dark pigments derived from the aromatic amino acid tyrosine [5]. The cuticle is known to confer multiple advantages against biotic stress, including fungal pathogens [6], predators [6], and bacteria [7,8], thus increasing the weevil fitness and danger for agriculture. Furthermore, the cuticle is also an efficient protective barrier against abiotic stress, including desiccation – the most important challenge faced by store grain pests [9]. Importantly, several insects thriving on substrates poor on aromatic amino acids

* Corresponding author.
** Corresponding author.
E-mail addresses: virginie.lacotte@insa-lyon.fr (V. Lacotte), pedro.da-silva@insa-lyon.fr (P. Da Silva).
[1] these authors contributed equally to this work.

https://doi.org/10.1016/j.heliyon.2023.e13962
Received 25 November 2022; Received in revised form 10 February 2023; Accepted 16 February 2023
Available online 23 February 2023

have established long term symbioses with bacterial partners that can synthesize them autotrophically, so that the excess can be redirected by the host to the biosynthesis of the cuticle building blocks. This is the case for several *Sitophilus* species [10], the red palm weevil *Rhynchophorus ferrugineus* [7], the sawtoothed grain beetle *Oryzaepilus surinamensis* [11], and many others [9]. In particular, the cereal weevil *Sitophilus oryzae* has been shown to harbor a population of gut endosymbionts of the gamma proteobacterium *Sodalis pierantonus,* whose presence improves cuticle darkening and thickening in young adult insects compared to aposymbiotic weevils (*i.e.* insects artificially devoid of endosymbionts) [10,12]. Because of its central role on beetle physiology and ecology, and its importance in driving the evolution of bacterial symbioses, proper evaluation of cuticle morphology and biosynthesis is of primary importance, both at the biochemical (composition) and at the mechanical level (color, thickness, and other physical properties).

The most common method of cuticle analysis to assess phenotypic changes involves qualitative visual picture observations [13–17]. This empirical observation is limited to changes that the human eye can detect, leading to a risk of missing important information, user error and assertion bias. For this reason, optical methods for insect cuticle characterization using a quantitative approach are gradually developing [18–20] and include: i) red, green, and blue color (RGB) quantification, ii) confocal microscopy, iii) electron microscopy, iv) spectroscopic-based methods, and v) hyperspectral imaging.

RGB composition analysis is a fast and simple method for quantifying color changes in insects, requiring common sample preparation and using basic equipment. Moreover, it is possible to use live insects, which is an asset to study an insect population over a long period of time, or to optimize timing of subsequent destructive measures [18]. Easy-to-use tools have been developed such as the ForensiGraph® (a grey and colored label added to each sample before image acquisition for RGB calibration [21]), or the *Natsumushi* software for RGB quantification [22]. For its versatility and easiness, RGB analyses have been used to study phenotypic changes related to the environment [21], gene expression [23] or even symbiotic relationships [12,24–27]. These changes can be assessed by quantifying, from digital images, the composition of RGB colors of the insect cuticle. Nevertheless, RGB analysis has some limitations. When taking images, there is no reference to standardize lighting conditions across all images. All photographs should therefore be taken under the same lighting conditions, ideally at the same time. Additionally, the lumpy and waxy surface of insect cuticles can create shiny or shadowy effects that compromise color analysis. Finally, this method which summarizes the surface color in only three colors has a limited precision to evaluate the complexity of the properties and color patterns of the cuticle, which can vary according to the area of the body, and from one insect to another.

Analysis of the composition and physical properties of dissected cuticles of arthropods is usually performed using Confocal Laser Scanning Microscopy (CLSM) [28–30], Scanning Electron Microscopy (SEM) [31,32], or Transmission Electron Microscopy (TEM) [33,34] coupled with a spectrophotometer. The CLSM technology measures the natural or induced fluorescence of the cuticle emitted in the RGB wavelengths of light. Using this technology, Eshghi et al. [30] have developed a simple, non-destructive imaging-based method to model the mechanical properties of insect cuticle with high efficiency compared to more complex mechanical methods [30]. However, the latter presents the same drawbacks as RGB analysis discussed above. The SEM and TEM coupled with a spectrophotometer have been used to study the structure of "metallic" gold and silver reflects on insect cuticles illuminated with a circularly polarized light (CPL) [19,35]. The spectrophotometer, unlike RGB analysis, makes it possible to measure the fraction of light energy reflected by insects, called reflectance, in a wider range of wavelengths, generally from 300 to 2500 nm, covering a part of ultraviolet, visible and near infrared light. Thus, it can measure the chemical signature of samples in response to light absorption by organic molecules [36]. Few studies have explored the potential of such spectrophotometer to classify insects according to their species [37], age, and gender but also to detect signs of infection [36]. In these cases, only the spectrophotometer is required to capture the light reflectance emitted by an insect, dead or alive, placed under the lens. This is called Near Infrared Spectroscopy (NIRS), but due to the lack of calibration, it is best to capture all samples under the same lighting conditions for comparisons. In addition, spectrophotometers generally focus on a few relatively broad wavebands between 300 and 2500 nm, which considerably reduces the information collected. Finally, background control is limited with spectrometry-based techniques, which requires zooming on smaller areas of the sample to avoid (or limit) background presence.

The newest optical technology that has been applied to insect cuticle analysis is Hyperspectral Imaging (HSI). A hyperspectral image is a hypercube composed by the spatial X and Y axes, and a spectral Z axis covering a broad range of wavelength, so that each pixel of the image contains a full wavelength information. It is then possible to select the area of interest in an image and extract its spectral signature at high-resolution. The HSI dataset can be processed with machine learning classifiers to extract the relevant information and develop more or less automated programs capable of detecting subtle changes in body reflectance with high accuracy. It is also a non-destructive method, making it possible to analyze the cuticle of living insects. Only few studies using HSI have been conducted so far, but it has already proven its great potential for monitoring phenotypic changes after insecticide exposure [38,39], comparing structural properties of insect cuticle and biomimetic film [40], and classifying insect species [41] and ages [42,43].

In comparison with the RGB method mostly used in optical analysis of insect cuticles, HSI has many advantages. First, each hyperspectral image is taken with a dark and white reference for calibration, making it possible to normalize the insect reflectance across samples, and therefore to capture images at any time and with different light parameters. Moreover, the high resolution of the data coupled with a statistical analysis makes it possible to cluster the insect cuticle pixels that constitute the shiny, shaded, neutral area or even more precisely the cuticle color patterns of certain species. Thus, we can record the average spectrum of a cluster of insect's pixels by avoiding areas of shadow or shine, and study the spectral signatures of complex structures and patterns of the insect cuticle.

No study has compared RGB and HSI methods on insects cuticle characterization but some performed on agricultural crops have shown that HSI was more reliable in phenotyping wheat crops [44] and more accurate in monitoring changes in storage feed quality over time [45,46] compared to RGB. Thus, the objective of this study is to evaluate the reliability and feasibility of HSI to analyze cereal weevil phenotypes and the possibility of use it as a standardized, simple, and automated analysis tool. To this end, we compared

the results obtained to monitor the phenotypic changes of symbiotic and aposymbiotic cereal weevils exposed to different nutritional stresses using the RGB quantification and HSI. Finally, we evaluated the practical application and the potential for standardization and automation of the two methods in laboratory conditions.

2. Materials and methods

2.1. Insect rearing and growth conditions

S. oryzae weevils [47] are reared in the dark at 27 °C and 70% relative humidity. Insects are routinely reared on organic wheat grains (Nature et Progrès®, Alès, France) kept at −80 °C to avoid grain contamination with mites. The aposymbiotic line was previously obtained by a heat treatment at 35 °C and 90% relative humidity for 1 month, followed by female oviposition under normal conditions, and maintained ever since [48]. Pupae were manually extracted from grains and subsequently kept on plates at 27 °C and 70% relative humidity until reaching stage 3 of adult development as in a previous study [12]. Note that in our conditions stage 1 is defined as the first adult stage after metamorphosis; adult stage 2 occurs 6–12 h after stage 1 and adult stage 3 occurs 12–24 h after stage 2; each developmental stage from stage 3 to stage 15 corresponds to a solar day. Subsequently, insects were pooled and subjected to various nutritional treatments.

To assess the potential of HSI in detecting cuticle color changes during development and depending on rearing conditions, we applied the HSI system to weevils subjected to some of the treatments investigated in Dell'Aglio et al. [12]. These conditions included: i) symbiotic weevils fed on wheat grains from adult stage 3 (control condition), ii) aposymbiotic weevils fed on wheat grains from adult stage 3, iii) symbiotic weevils fed on wheat grains from adult stage 5, and iv) symbiotic weevils fed on starch grains (Stijfsel Remy, Belgium), from adult stage 3. In all conditions, the pools of weevils were maintained up to adult stage 15.

2.2. Sample preparation

For the RGB analysis of weevils' cuticle performed previously [12], 20 to 30 weevils per conditions were used. At every capture day, 8 to 15 randomly selected living individuals were imaged from each pool. Regarding hyperspectral images taken during this study, 8 to 20 individuals were collected at each condition and stage. They were frozen and kept at −80 °C until imaged.

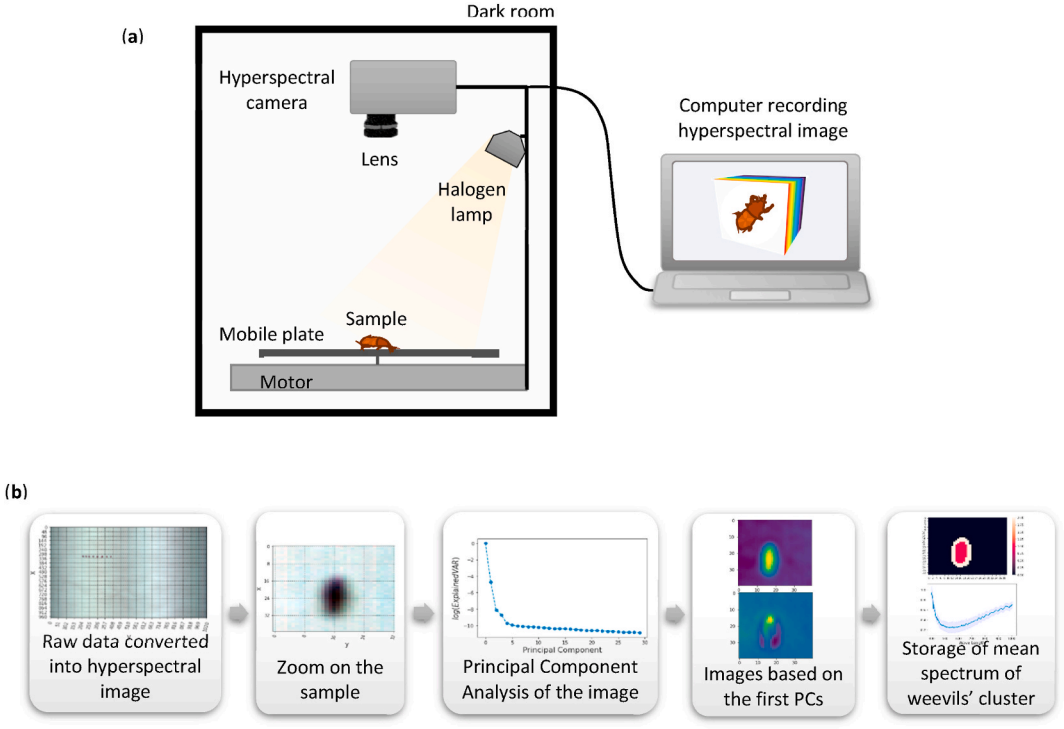

Fig. 1. Hyperspectral images acquisition and analysis. (a) Pushbroom Hyperspectral Imaging system for hyperspectral images recording combining a spatial and spectral dimension. The spatial and spectral axis form a hypercube; (b) Hyperspectral images processing resulting in a weevil spectral library. Data conversion and statistical analysis are performed using a Jupyter notebook script. Adapted from Lacotte et al. [50].

2.3. Analysis of cuticle color using RGB method

Data for weevil cuticle tanning obtained with the RGB method have been published previously [12]. Briefly, the analysis was performed with the method described in Tanahashi et al. [22] and used in other studies [24–27]. Color digital images were taken with an Olympus XC50 (Olympus LS, Tokyo, Japan) camera attached to a Leica MZFLIII (Leica Camera AG, Wetzlar, Germany), binocular and the *CellF* software (Olympus Soft Imaging System). As the normalization of the digital images is not feasible, all the images were carefully taken in the same lighting conditions and keeping the samples at the same distance of the device. Cuticle tanning was then evaluated with the software *Natsumushi* v.1.10 (National Institute of Advanced Industrial Science and Technology (AIST), Tsukuba, Japan) for entomological studies, using thorax redness as a proxy calculated as Σ (R – mean [R, G, B])/n (n = each measured pixel), as described in Anbutsu et al. [26]. The thorax region was selected for its uniformity in color with respect to the abdomen, especially at late adult stages. Because the weevils' cuticle unevenness creates shiny spots and shadows on the surface, we excluded the pixels with brightness over top 10% or below bottom 10%. Data are reported as mean and standard error per condition and stage.

2.4. Analysis of cuticle reflectance by hyperspectral imaging

2.4.1. Hyperspectral image recording

Images were acquired using a pushbroom HSI system (Fig. 1a) composed of a HSI camera Specim FX10 (Specim, Spectral Imaging Ltd., Oulu, Finland) and a halogen lighting mounted above a mobile plate Specim LabScanner (Specim, Spectral Imaging Ltd., Oulu, Finland). The HSI system is controlled from a computer recording the hyperspectral image using Specim's *LUMO Scanner* software (Specim, Spectral Imaging Ltd., Oulu, Finland). The camera has a spectral range of 400–1000 nm, corresponding to the visible (400–700 nm) and Near Infrared – NIR (700–1000 nm) region of the light spectrum. Along the mobile plate, we can record a hyperspectral image with a camera line of 1024 spatial pixels and a spectral data acquisition along this line with a maximum frame rate of 327 frames per second (fps) full frame. During the image capture, the camera parameters were as follows: RGB calibration on 700, 535 and 436 nm respectively; frame rate at 50 Hz; exposure time at 10 ms and scanning speed at 10 mm/s with a positioning speed of 40 mm/s.

Before taking the hyperspectral images, frozen weevils were thawed for a few minutes and their cuticle wiped to prevent the water condensed on the surface from impacting the reflection of light. Then, weevils were staged on their abdomen on a white paper background, and their cuticle reflectance was captured. During hyperspectral measurements, the HSI system was placed in a black room to avoid interferences with other light sources than halogen lamps. Each hyperspectral image was taken with two extra images for reflectance calibration, the dark reference recorded by closing an internal camera shutter and the white reference recorded on a Teflon white calibration bar with standard reflectance of 99%. One hyperspectral image containing all weevil replicates was taken per stage and condition. Weevil hyperspectral images are publicly available at Lacotte et al. [49].

2.4.2. Image processing

Hyperspectral image processing was performed as in Lacotte et al. [50] using a Jupyter Notebook Python 3.7 script [51], relying on the scikit-learn [52], Pandas [53], Numpy [54], Matplotlib [55], Seaborn [56] and Spectral [57] Python libraries. The Jupyter Notebook script used in this work is also publicly available at Lacotte et al. [49]. For each hyperspectral image, first, we converted the raw data into a hyperspectral reflectance image and manually zoomed on the weevils one by one, performing the following steps for each replicate (Fig. 1b).

On the zoomed image containing one weevil, we applied a Principal Component Analysis (PCA) [58] of the spectra and computed the percentage of variance carried by each Principal Component (PC). Next, we visualized the zoomed image projected on the most important PCs and kept the PCs revealing the weevil for the remaining steps. Usually, the two first PCs were selected, revealing the weevil's body and the shadow surrounding it, respectively. Afterwards, we applied a K-means clustering algorithm [59] on the pixels of the zoomed image projected in the kept PCs space, in order to group similar pixels together. Thus, we generally obtained three clusters corresponding to the weevil, its shadow, and the background. Finally, we computed the average spectrum of the pixels corresponding to the weevil's cluster, normalized the raw data using dark and white references to show light reflectance spectrum between 0 (minimum reflectance) and 1 (maximum reflectance) and stored it in a dataset.

2.4.3. Cuticle reflectance analysis

Before analyzing weevil cuticle reflectance, an Isolation Forest technique [60] was used to remove outliers from the normalized weevil spectra dataset. Then, for each developmental stage, we computed the average and standard deviation of the light reflectance spectra between 400 and 1000 nm, as represented in Fig. 3. The average spectra for the different developmental stages share the same profiles, differ mainly in terms of reflectance intensity, especially for wave lengths higher than 600 nm. Then, in order to assess the reflectance as a function of the developmental stage, we computed the total reflectance as the sum of reflectance values within the most discriminating wavelength region. To do so, we compute for each wavelength λ the inter-condition Sum of Square Errors (SSE^{λ}_{inter}). Let $x^{\lambda}_{i,c}$ be the reflectance of spectrum i of cuticle tanning condition c (i.e., both rearing condition and developmental stage considered simultaneously), along wavelength λ. Let $\overline{x^{\lambda}_{c}} = \frac{1}{n_c}\sum_{i=1}^{n_c} x^{\lambda}_{i,c}$ be the average reflectance for condition c along wavelength λ and let $\overline{x^{\lambda}_{c}} = \frac{1}{N}\sum_{c=1}^{C}\sum_{i=1}^{n_c} x^{\lambda}_{i,c}$ denote the average reflectance along wavelength λ where n_c denotes the number of reflectance values of condition c and $N = \sum_{c=1}^{C} n_c$ denotes the total number of reflectance values. Then, the inter-condition Sum of Square Errors for wavelength λ is defined

as $SSE^{\lambda}_{inter} = \sum_{c=1}^{C} n_c(\overline{x^{\lambda}_c} - \overline{x^{\lambda}})^2$. In order to determine the most discriminating wavelength region, we have computed the inter-condition Sum of Square Errors for all wavelengths, then we computed the 66th percentile denoted SSE^*, and finally, we determine the discriminating wavelength region Λ such that for all $\lambda \in \Lambda$, $SE^{\lambda}_{inter} \geq SSE^*$. In this work, the region Λ falls between 690 and 900 nm (Fig. 2).

3. Results and discussion

3.1. Weevil's hyperspectral reflectance

The cuticle of symbiotic *S. oryzae* weevils has been shown to darken and thicken in early adults [10]. By using the decrease in thorax redness as a proxy for cuticle reinforcement in a RGB quantification, we have shown that cuticle darkening occurs from adult stage 1 to adult stage 9 (defined as in Dell'Aglio et al. [12] as different phases after larval metamorphosis, see Methods and Fig. 3), while in the following stages no more differences are observed [12]. A surplus of aromatic amino acids produced by *S. pierantonius* gut endosymbionts has been shown to be crucial for physiological cuticle reinforcement [10], thus explaining the lighter and thinner cuticle of aposymbiotic weevils [10,12] (Fig. 3).

To compare the previously employed RGB quantification technique with HSI, we performed statistical analysis on hyperspectral images data and obtained a database listing the normalized average reflectance spectrum from 400 to 1000 nm of weevils per condition and developmental stage (Fig. 4a). Weevil's spectral signatures showed a high absorbance of short high-energy wavelengths, corresponding to the purple-blue range of the visible light (400–500 nm), then an increasingly reflectance of larger wavelengths at low energy, corresponding to the green-red range of the visible light (500–700 nm) and the NIR range (700–1000 nm). The same reflectance parameters have already been observed in other beetles such as *Chrysina aurigans* [34]. The presence of melanin pigments in weevil cuticle layers might explain this high absorption of short wavelengths as light absorption by melanin increases with decreasing wavelength, especially when approaching the violet wavelength range [34]. Moreover, although very little is known on NIR insect reflectance, the high reflectance in the NIR range could be the consequence of multiple scattering inside intercellular spaces in the weevil body [61]. Globally, the spectral curves from all stages have the same pattern but different levels of light reflectance. Indeed, the more the weevil's cuticle tans over time (Fig. 3), the lower the light reflectance (Fig. 4a) as light colors reflect light more than dark ones.

The spectral signatures measured by HSI correspond to empirical observations of *S. oryzae*'s cuticle tanning, confirming the potential of such an approach for weevil's cuticle analysis in comparison with the usual RGB method. However, the graphic representation of the weevil's reflectance spectra does not allow an efficient analysis of the information since the curves, which can be numerous when comparing several conditions, overlap and prevent correct visualization of the differences in reflectance. Therefore, since the difference between the weevil spectra was mostly in the overall reflectance level, we summed the reflectance values in the most discriminating wavelength region and visualized the total reflectance of each developmental stage (Fig. 4b). The weevils' cuticle tanning, corresponding to a decrease in total reflectance, occurs suddenly between stages 1 and 3, then gradually up to stage 15. Thus, hyperspectral imaging can assess cuticle changes between different stages of development and makes it possible to compare in the following section results of total reflectance of weevils of all stages and conditions with those obtained by RGB quantification [12].

3.2. The new HSI-based cuticle analysis method mirrors RGB-based standard method in a variety of developmental and stress conditions

Next, we analyzed the changes in cuticle reflectance for symbiotic and aposymbiotic weevils as well as weevils subjected to different diets, and we compared our results based on total reflectance, obtained by HSI on the whole insect body, with previous thorax

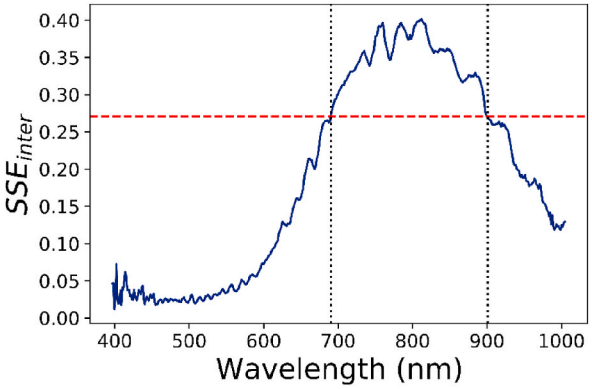

Fig. 2. Inter-condition Sum of Squared Errors for each wavelength. The 66th percentile is denoted as a red line and the most discriminating wavelength region between 690 and 900 nm is delimited using vertical black lines. (For interpretation of the references to color in this figure legend, the reader is referred to the Web version of this article.)

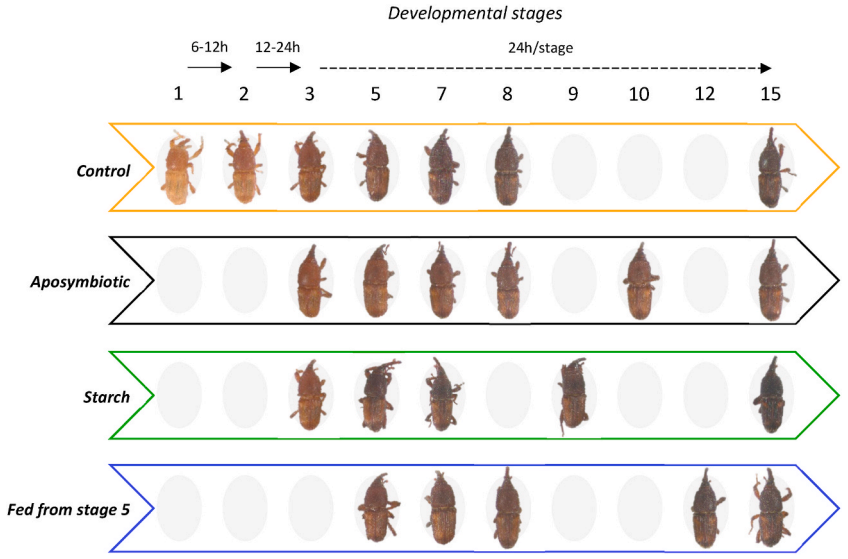

Fig. 3. Digital images of weevil's phenotypes per condition and stage. Adult weevils normally start feeding at stage 3. Here, both control and aposymbiotic weevils were fed from stage 3 onwards with wheat grains. Starch-fed symbiotic weevils were fed from stage 3 onwards but only with pure starch. Finally, a group of symbiotic weevils was fed on wheat grains only from stage 5 onwards. Cuticle tanning increases over time at a different rate depending on the conditions. The images were taken with an Olympus XC50 camera attached to a Leica MZFLIII binocular.

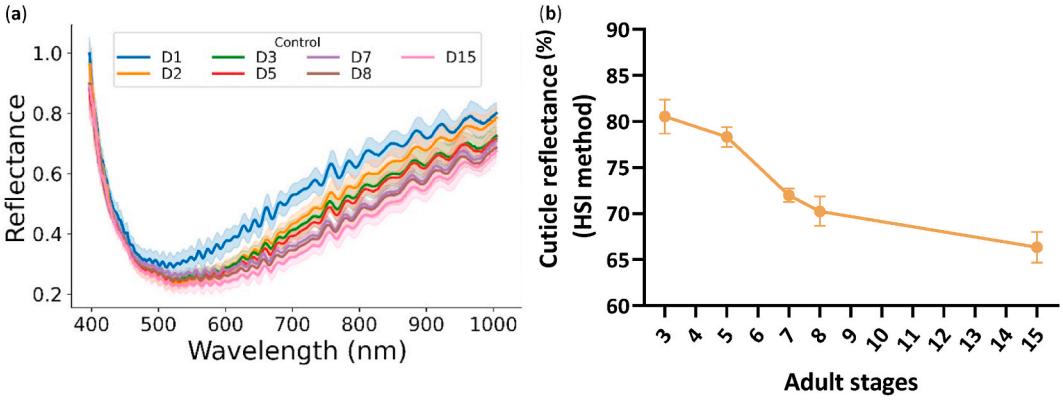

Fig. 4. Light reflectance of weevils from the control condition measured by Hyperspectral Imaging. (a) Normalized average light reflectance spectra with standard deviation between 400 and 1000 nm. Light reflectance decreases with developmental stages (D1 to D15), along with cuticle tanning. (b) Average total reflectance (%) of each developmental stage of the control weevils calculated by the sum of reflectance values in the most discriminating wavelength region between 690 and 900 nm. Error bars represent standard error. The weevils' cuticle tanning corresponds to a decrease in total reflectance.

redness quantifications obtained by the RGB method [12] (Fig. 5). The thorax redness curves based on RGB analysis (Fig. 5b,d,f) and those of total reflectance obtained by HSI (Fig. 5a,c,e) have the same pattern. Therefore, the decrease in weevil thorax redness and total reflectance correlate with cuticle tanning across developmental stages (Figs. 3 and 5).

First, in agreement with RGB-based results [10,12], the HSI-based method shows that aposymbiotic insects are impaired in cuticle development, which is slower than symbiotic insects and the profiles obtained with the two techniques are similar (Fig. 5a–b). In particular, the lowest aposymbiotic weevil's thorax redness index is equivalent to that of symbiotic weevils at stage 7. Consequently, aposymbiotic weevils never complete their cuticle tanning. Thus, HSI-based results (Fig. 5a) corroborate the previous conclusions (Fig. 5b) [12] that endosymbionts are crucial for weevil's cuticle tanning.

We then decided to test our HSI-based method by following the cuticle tanning of symbiotic weevils subjected to nutritional stress. Firstly, we analyzed cuticle development in insects fed from stage 3 only with pure starch. These weevils showed a faster cuticle tanning process (Fig. 5c), mirroring previous results obtained with the standard RGB-based method (Fig. 5d) [12,26] and might be due to the higher friability of starch grains, which could be easier to eat and digest than wheat grains, thus leading to a faster energy uptake by the insect as well as to symbiotic bacteria which might contribute more to cuticle biosynthesis.

Finally, we tested the effects of feeding symbiotic weevils only from stage 5 onwards instead of from stage 3 onwards. The two-days

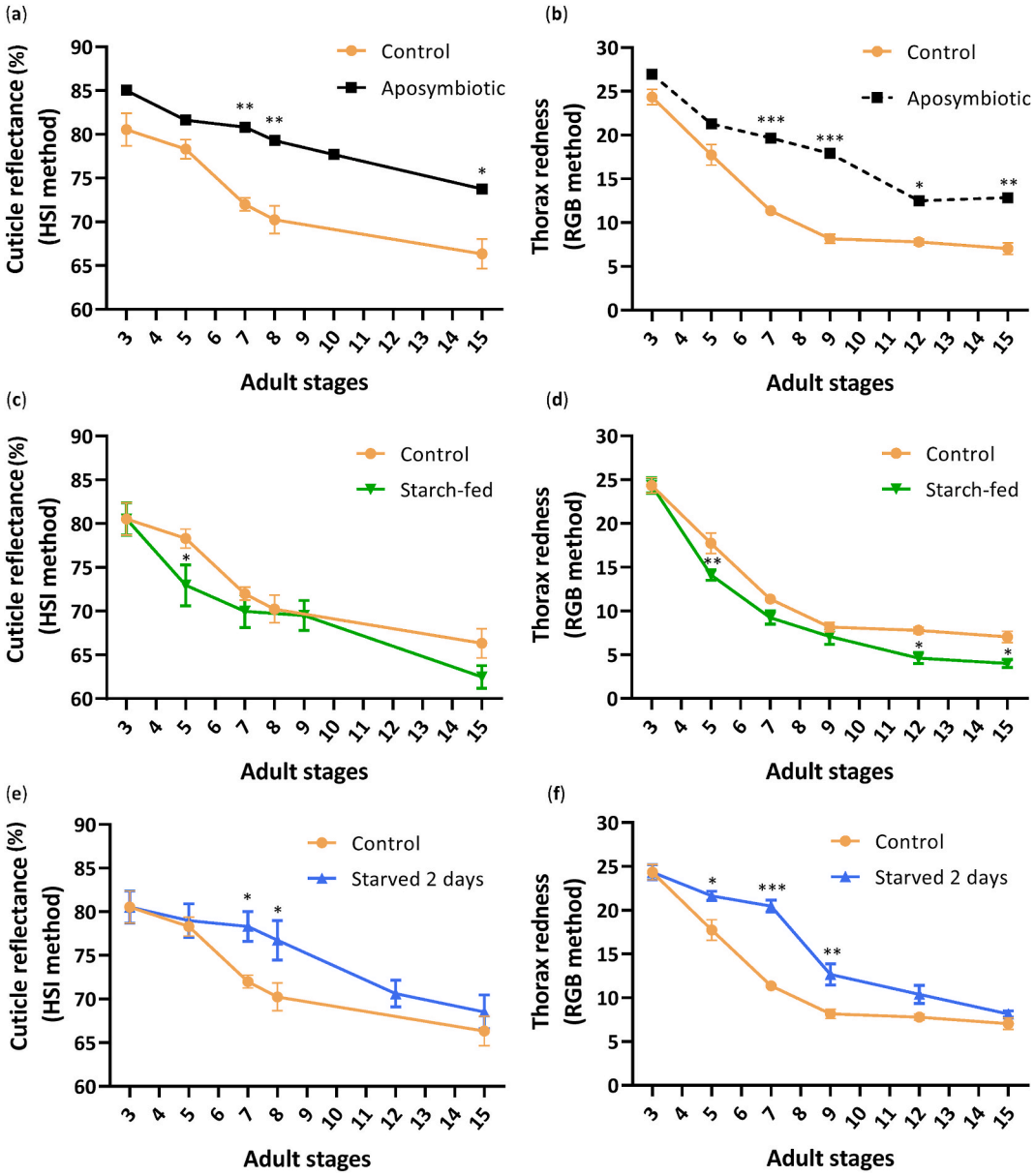

Fig. 5. Quantitative evaluation of phenotypic changes in weevils exposed to nutritional stresses by optical methods. (a,b) Cuticle darkening process measured in symbiotic (control) and aposymbiotic adult weevils by the HSI method and RGB method, respectively. (c,d) Cuticle darkening process measured in symbiotic (control) and starch-fed adult weevils by the HSI method and RGB method, respectively. (e,f) Cuticle darkening process measured in symbiotic (control) and starved adult weevils by the HSI method and RGB method, respectively. Data for thorax redness evaluation by RGB are taken from Dell'Aglio et al. [12]. RGB values for all (=n) pixels were measured and averaged to obtain the thorax redness index without unit by Σ (R − mean [R, G, B])/n. The cuticle average total reflectance (%) per developmental stage and condition is calculated by the sum of the reflectance values in the most discriminating wavelength region between 690 and 900 nm. Error bars represent standard error of the mean. Comparisons were made by two-way ANOVA followed by Tukey's multiple comparison test. *: $p < 0.05$, **: $p < 0.01$; ***: $p < 0.001$. The weevils' cuticle tanning corresponds to a decrease in thorax redness and total reflectance.

starvation period was associated, with both RGB and HSI-based methods, with a significant delay in cuticle tanning compared to the control fed from stage 3 (Fig. 5e–f). The thorax redness as well as the total cuticle reflectance of starved weevils are superposable from stage 3–7, then the cuticle tanning was triggered and let to a phenotype similar to the control from stage 12 onwards [12]. This suggests that nutrient supply is crucial to maintain endosymbiont proliferation, thereby supporting the cuticle tanning process. In agreement with the previous RGB-based results (Fig. 5f), our HSI-based method showed a clear delay in cuticle tanning of starved insects at stages 7 and 8, with subsequent recovery at stage 12 and 15 (Fig. 5e).

These subtle phenotypic changes in weevils exposed to nutritional stresses have been successfully detected and quantified using

Table 1
Comparative study of Red-Green-Blue (RGB) and Hyperspectral Imaging (HSI) technologies for image analysis in laboratory conditions based on current knowledge [62–69]. Scores are assigned from 1 (low) to 4 (high) points on various features such as the cost of the equipment, the quality as well as the ease of acquisition and analysis of the data and the precision of the results. The text in italics refers to the equipment used in this study while the regular text refers to general information related to RGB and HSI technologies.

Feature		RGB	HSI
Technology	Equipment	Digital camera + (optical microscope) + computer	Hyperspectral camera + scanner + computer
	Model example	*Olympus XC50 camera + Leica MZFLIII binocular*	*HSI camera Specim FX10 + Specim LabScanner*
	Price	■	■■■
	Portability	■■■■	■■
	Storage space required	■	■■■
Data quality	Spatial information	✓	✓
	Spatial resolution	*72 ppi*	*130 ppi*
	Color information RGB	✓	✓
	Color depth	*24 bits/px*	*12 bits/px*
	Spectral information	×	✓
	Spectral resolution	×	*5 nm* (1-10 nm)
	Spectrum beyond visible light	×	*400-1000 nm* (Infrared 700-2500)
	Information amount	■	■■■■
	Image size	*15 Mb*	*1 Gb*
	Multi-constituent information	Limited	✓
	Sensitivity to minor components	×	✓
Data acquisition	Current expertise	■■■	■
	Usability	■■■	■■
	Noninvasive	✓	✓
	Lighting homogeneity	■	■■■
	Lighting calibration	×	✓
	Standardization	■	■■■
	Image speed	*24 fps*	*327 fps* High speed for large data recording. Depends on scanner speed.
Data analysis	Software available	Commercial software and others created by peers	Vendors software
	Software application scope	■■■	■
	Custom software development	■	■■■
	Machine learning approach	■	■■■ Suitable for processing of large data
	Computing power required	■	■■■
	Analysis speed	■■■	■ Depends on computing power. Faster once the technique is established.
	Automation	■	■■ High automation potential but more training and expertise required
Results	Interpretation	■■■	■■ Deeper knowledge of spectral data with transdisciplinary cooperation required for robust analysis tools
	Abiotic and biotic stress detection	■■	■■■
	Early changes detection	■	■■■
	Storage food quality control	■	■■■
	Accuracy	■■ Depends on color mixing and image quality. Limited by factors interacting.	■■■■

optical analysis methods (Fig. 5), which would not have been possible by a simple visual qualitative analysis of cuticles (Fig. 3). Moreover, the agreement between the previously employed RGB quantification of thorax redness and present measurements of total reflectance by HSI demonstrate that HSI is a reliable method for the phenotypic analysis of weevils, in a variety of growth and stress conditions.

3.3. Comparison of the use of hyperspectral imaging versus RGB technologies in laboratory conditions

Having demonstrated the reliability of HSI for detecting phenotypic changes in weevil cuticle, the feasibility of widespread use of this technology in cuticle research through a simple, accessible, standardized, and automated analysis tool should be assessed. To evaluate the possibility of developing such a tool, we compared the use of HSI and RGB technologies in laboratory conditions on many practical aspects such as the equipment investment, the quality as well as the ease of acquisition and analysis of the data and the precision of the results (Table 1).

The equipment for HSI consists of a hyperspectral camera coupled with a scanner moving under the camera lens and a computer for recording and analyzing the images [62]. This equipment is similar to that of RGB analysis which includes a digital camera, a microscope for the analysis of small samples, and a computer. The main difference is the available budget since, although the HSI is not excessively expensive and is spreading in the market becoming more accessible, it remains considerably more expensive than the RGB technology which can consist of a simple camera or even a phone [62–65]. The portability of RGB technology can thus be much higher than with HIS [64]. However, this is no longer true if one uses a microscope coupled to the camera to observe details in small samples, as in this study.

Both technologies transmit spatial and color information (RGB) related to the analyzed sample but only the HSI provides spectral information [66]. According to the properties of the models used in this study (Table 1), the HSI technology has a lower color depth than the RGB technology (12 bits/px against 24 bits/px), but a higher spatial definition (130 ppi against 72 ppi) and a very high spectral resolution (5 nm on average) providing information in visible light and well beyond (from 400 up to 2500 nm, including visible, near and short-wave infrared) [64,67,68]. This large amount of information collected with HSI (image of 1 Gb against 15 mb with RGB technology) makes it possible to analyze the multiple constituents of an image as well as its minor components, which is hardly possible with the RGB method [66].

Image acquisition with the RGB method is well understood while very little is known about HSI in research [63,64]. However, both are easy to use and do not require complex sample preparation, which can even be live animals, as imaging is non-invasive [64,68]. For both technologies, the image acquisition parameters must be set before shooting. Then it is possible to capture a series of images with the same parameters. With the RGB method, it will be necessary to configure the focus, sharpness, lighting, and distance between the sample and the sensor because all these characteristics influence the image quality and therefore the precision of the results [69]. Then, image capture is relatively fast with a speed of 24 fps with the model used in this study.

Since there is no lighting calibration, special attention must be given to the image configuration step to repeat the results, otherwise all images must be taken at the same time [69]. By using HSI, it will be necessary to define parameters on the camera and the scanner which will always remain the same such as the frame rate or the scan speed. Then, images are taken at a high speed of 327 fps (with the camera used) allowing the recording of a large amount of data in a few seconds. For each image, the lighting is calibrated by recording a black and white reference. Calibration makes it possible to compare images taken under different lighting conditions and at different times and opens up the possibility to develop a standardized imaging procedure [62].

Image analysis is done using software developed by vendors or by peers [63,69]. In the case of RGB analysis, several easy-to-learn software exist with a very wide scope for analyzing various objects, colors, and shapes. Automated image analysis is possible but difficult due to heterogenic lighting conditions and image quality [69]. There is little software for the analysis of hyperspectral images which are often created by suppliers for very specific uses depending on the type of sample and the element detected. Thus, the development of custom software for hyperspectral image analysis is booming. This software generally incorporates machine learning that is perfectly suited to processing the large amounts of data provided by HIS [64,65,68]. Running the software requires a lot of computing power on which the speed of data analysis will depend [62,64]. Furthermore, the use of machine learning opens the door to the automation of data analysis [62,63], that can be based on a technique established by experts including data dimensioning and extensive training, increasing at the same time the speed of analysis [64].

The interpretation of the results of RGB analysis based on the color of the samples is relatively simple, while that of hyperspectral images based essentially on spectral information requires interdisciplinary expertise to associate a light response with a biological or chemical status [68]. This last point requires deeper knowledge in order to develop robust cuticle analysis tools that can be used by everyone [65,67]. Thus, with proper use of this technology, HSI has the potential to detect with high accuracy abiotic or biotic stresses, early phenotypic changes or monitor storage food infestation [64].

4. Conclusions

Here, we showed for the first time the reliability and feasibility of HSI as a tool for standardized analysis of cuticle changes in weevils under different diets throughout their development. HSI technology is increasingly available, and is easy to use under laboratory conditions. HSI provides the image calibration required for a standardized imaging process, so that the initial cost can be quickly offset by the productivity benefits for a wide range of projects and purposes. In addition, it provides high quality data in large quantities, enabling the development of machine learning based software that can lead to the automation of data analysis. HSI seems to be the best technology for the development of an analysis tool in entomological research, which could be achieved in the future.

The development and standardization of such an HSI analysis tool will require the definition of a standardized imaging procedure based on the same camera and scanner parameters, as well as the use of samples produced under the same conditions, whether they are live, dead, frozen, dissected or whole, depending on the needs of the study. It would then be possible to develop automated software to detect insects in images, record their spectral signature, classify them on the basis of their spectral differences and associate them with a species, genus, age or even stress, as previously reported [37,38,40–42]. To develop a robust tool to accurately and comprehensively reconstruct the properties and changes of insect cuticles, a large amount of data and the collaboration of several bioinformatics, photobiology and entomology researchers would be required, to allow a wide dissemination of the HSI technology [65,68].

Author contribution statement

Virginie Lacotte, Elisa Dell'Aglio and Sergio Peignier: Conceived and designed the experiments; Performed the experiments; Analyzed and interpreted the data; Wrote the paper.

Fadéla Benzaoui: Performed the experiments; Analyzed and interpreted the data.

Rita Rebollo: Conceived and designed the experiments; Analyzed and interpreted the data.

Abdelaziz Hedd: Conceived and designed the experiments; Wrote the paper.

Pedro DA SILVA: Conceived and designed the experiments; Analyzed and interpreted the data; Wrote the paper.

Funding statement

Rita Rebollo was supported by Agence Nationale de la Recherche [UNLEASH-ANR-CE20-0015-01].

Pedro DA SILVA was supported by Agence Nationale de la Recherche [ANR-17-CE34-0012-03].

Data availability statement

Data associated with this study has been deposited at Weevil hyperspectral images database. (2022) https://doi.org/10.57745/PNWEWS.

Declaration of interest's statement

The authors declare that they have no known competing financial interests or personal relationships that could have appeared to influence the work reported in this paper.

Acknowledgements

The authors are grateful to Patrice Baa-Puyoulet for his great help in publishing the database online.

References

[1] I.P.P.C. Secretariat, Scientific Review of the Impact of Climate Change on Plant Pests: A Global Challenge to Prevent and Mitigate Plant-Pest Risks in Agriculture, Forestry and Ecosystems, FAO on behalf of the IPPC Secretariat, Rome, Italy, 2021, https://doi.org/10.4060/cb4769en.

[2] R. Zunjare, F. Hossain, V. Muthusamy, S.K. Jha, P. Kumar, J.C. Sekhar, N. Thirunavukkarasu, H.S. Gupta, Genetic variability among exotic and indigenous maize inbreds for resistance to stored grain weevil (Sitophilus oryzae L.) infestation, Cogent Food Agric 2 (2016), 1137156, https://doi.org/10.1080/23311932.2015.1137156.

[3] T.T. Nguyen, P.J. Collins, P.R. Ebert, Inheritance and characterization of strong resistance to phosphine in Sitophilus oryzae (L.), PLoS One 10 (2015), e0124335, https://doi.org/10.1371/journal.pone.0124335.

[4] R. Kaur, M. Subbarayalu, R. Jagadeesan, G.J. Daglish, M.K. Nayak, H.R. Naik, S. Ramasamy, C. Subramanian, P.R. Ebert, D.I. Schlipalius, Phosphine resistance in India is characterised by a dihydrolipoamide dehydrogenase variant that is otherwise unobserved in eukaryotes, Heredity 115 (2015) 188–194, https://doi.org/10.1038/hdy.2015.24.

[5] M.Y. Noh, S. Muthukrishnan, K.J. Kramer, Y. Arakane, Cuticle formation and pigmentation in beetles, Curr. Opin. Insect Sci. 17 (2016) 1–9, https://doi.org/10.1016/j.cois.2016.05.004.

[6] S.N. Kanyile, T. Engl, M. Kaltenpoth, Nutritional symbionts enhance structural defence against predation and fungal infection in a grain pest beetle, J. Exp. Biol. 225 (2022) jeb243593, https://doi.org/10.1242/jeb.243593.

[7] A. Muhammad, P. Habineza, T. Ji, Y. Hou, Z. Shi, Intestinal microbiota confer protection by priming the immune system of red palm weevil Rhynchophorus ferrugineus olivier (Coleoptera: dryophthoridae), Front. Physiol. 10 (2019). https://www.frontiersin.org/articles/10.3389/fphys.2019.01303 (accessed August 4, 2022).

[8] Y. Wang, D.E. Rozen, Gut microbiota in the burying beetle, Nicrophorus vespilloides, provide colonization resistance against larval bacterial pathogens, Ecol. Evol. 8 (2018) 1646–1654, https://doi.org/10.1002/ece3.3589.

[9] T. Engl, N. Eberl, C. Gorse, T. Krüger, T.H.P. Schmidt, R. Plarre, C. Adler, M. Kaltenpoth, Ancient symbiosis confers desiccation resistance to stored grain pest beetles, Mol. Ecol. 27 (2018) 2095–2108, https://doi.org/10.1111/mec.14418.

[10] A. Vigneron, F. Masson, A. Vallier, S. Balmand, M. Rey, C. Vincent-Monégat, E. Aksoy, E. Aubailly-Giraud, A. Zaidman-Rémy, A. Heddi, Insects recycle endosymbionts when the benefit is over, Curr. Biol. 24 (2014) 2267–2273, https://doi.org/10.1016/j.cub.2014.07.065.

[11] T. Engl, T.H.P. Schmidt, S.N. Kanyile, D. Klebsch, Metabolic cost of a nutritional symbiont manifests in delayed reproduction in a grain pest beetle, Insects 11 (2020) 717, https://doi.org/10.3390/insects11100717.

[12] E. Dell'Aglio, V. Lacotte, S. Peignier, I. Rahioui, F. Benzaoui, A. Vallier, P. Da Silva, E. Desouhant, A. Heddi, R. Rebollo, Weevil Carbohydrate Intake Triggers Endosymbiont Proliferation: A Trade-Off between Host Benefit and Endosymbiont Burden, mBio 0 (2023) e03333–03322, https://doi.org/10.1128/mbio.03333-22.

[13] L. Qiao, M. Du, X. Liang, Y. Hao, X. He, F. Si, T. Mei, B. Chen, Tyrosine Hydroxylase is crucial for maintaining pupal tanning and immunity in Anopheles sinensis, Sci. Rep. 6 (2016), 29835, https://doi.org/10.1038/srep29835.

[14] T.R. Lemonds, J. Liu, A. Popadić, The contribution of the melanin pathway to overall body pigmentation during ontogenesis of Periplaneta americana, Insect Sci. 23 (2016) 513–519, https://doi.org/10.1111/1744-7917.12356.

[15] M.-H. Du, Z.-W. Yan, Y.-J. Hao, Z.-T. Yan, F.-L. Si, B. Chen, L. Qiao, Suppression of Laccase 2 severely impairs cuticle tanning and pathogen resistance during the pupal metamorphosis of Anopheles sinensis (Diptera: Culicidae), Parasit, Vector 10 (2017) 171, https://doi.org/10.1186/s13071-017-2118-4.

[16] L.-J. Ze, P. Wang, Y.-C. Peng, L. Jin, G.-Q. Li, Silencing tyrosine hydroxylase or dopa decarboxylase gene disrupts cuticle tanning during larva-pupa-adult transformation in henosepilachna vigintioctopunctata, Pest Manag. Sci. (2022), https://doi.org/10.1002/ps.6948 n/a.

[17] S. Chen, S. Nanda, M. Guo, L. Kong, C. Yang, Z. Liu, R. Gao, B. Qiu, Y. Zhang, X. Zhou, H. Pan, Tyrosine Hydroxylase Involved in Cuticle Tanning and Reproduction in the 28-spotted Potato Ladybeetle, Henosepilachna Vigintioctopunctata, Pest Manag. Sci. (2022), https://doi.org/10.1002/ps.6980 n/a.

[18] C. Nansen, The potential and prospects of proximal remote sensing of arthropod pests: proximal remote sensing of arthropod pests, Pest Manag. Sci. 72 (2016) 653–659, https://doi.org/10.1002/ps.4209.

[19] A.C. Neville, Optical methods in cuticle research, in: T.A. Miller (Ed.), Cuticle Tech. Arthropods, Springer, New York, NY, 1980, pp. 45–89, https://doi.org/10.1007/978-1-4612-6076-9_2.

[20] C. Nansen, N. Elliott, Remote sensing and reflectance profiling in entomology, Annu. Rev. Entomol. 61 (2016) 139–158, https://doi.org/10.1146/annurev-ento-010715-023834.

[21] R.A. Stanbrook, W.E. Harris, C.P. Wheater, M. Jones, Evidence of phenotypic plasticity along an altitudinal gradient in the dung beetle Onthophagus proteus, PeerJ 9 (2021), e10798, https://doi.org/10.7717/peerj.10798.

[22] M. Tanahashi, T. Fukatsu, Natsumushi: image measuring software for entomological studies, Entomol. Sci. 21 (2018) 347–360, https://doi.org/10.1111/ens.12315.

[23] T. Bai, X. Pei, T. Liu, Y. Fan, S. Zhang, Melanin synthesis genes *BgTH* and *BgDdc* affect body color and cuticle permeability in *Blattella germanica*, Insect Sci. (2022) 1744–7917, https://doi.org/10.1111/1744-7917.13024, 13024.

[24] B. Hirota, G. Okude, H. Anbutsu, R. Futahashi, M. Moriyama, X.-Y. Meng, N. Nikoh, R. Koga, T. Fukatsu, A novel, extremely elongated, and endocellular bacterial symbiont supports cuticle formation of a grain pest beetle, mBio 8 (2017), https://doi.org/10.1128/mBio.01482-17 e01482-17.

[25] R. Koga, M. Moriyama, N. Onodera-Tanifuji, Y. Ishii, H. Takai, M. Mizutani, K. Oguchi, R. Okura, S. Suzuki, Y. Goto, T. Hayashi, M. Seki, Y. Suzuki, Y. Nishide, T. Hosokawa, Y. Wakamoto, C. Furusawa, T. Fukatsu, Single Mutation Makes Escherichia coli an Insect Mutualist, 2022, https://doi.org/10.1101/2022.01.26.477692, 2022.01.26.477692.

[26] H. Anbutsu, M. Moriyama, N. Nikoh, T. Hosokawa, R. Futahashi, M. Tanahashi, X.-Y. Meng, T. Kuriwada, N. Mori, K. Oshima, M. Hattori, M. Fujie, N. Satoh, T. Maeda, S. Shigenobu, R. Koga, T. Fukatsu, Small genome symbiont underlies cuticle hardness in beetles, Proc. Natl. Acad. Sci. USA 114 (2017), https://doi.org/10.1073/pnas.1712857114.

[27] J.S.T. Kiefer, S. Batsukh, E. Bauer, B. Hirota, B. Weiss, J.C. Wierz, T. Fukatsu, M. Kaltenpoth, T. Engl, Inhibition of a nutritional endosymbiont by glyphosate abolishes mutualistic benefit on cuticle synthesis in Oryzaephilus surinamensis, Commun. Biol. 4 (2021) 1–16, https://doi.org/10.1038/s42003-021-02057-6.

[28] S. Büsse, S.N. Gorb, Material composition of the mouthpart cuticle in a damselfly larva (Insecta: odonata) and its biomechanical significance, R. Soc. Open Sci. 5 (2018), 172117, https://doi.org/10.1098/rsos.172117.

[29] J. Michels, S.N. Gorb, Detailed three-dimensional visualization of resilin in the exoskeleton of arthropods using confocal laser scanning microscopy: detailed three-dimensional visualization of resilin, J. Microsc. 245 (2012) 1–16, https://doi.org/10.1111/j.1365-2818.2011.03523.x.

[30] S.h. Eshghi, M. Jafarpour, A. Darvizeh, S.N. Gorb, H. Rajabi, A simple, high-resolution, non-destructive method for determining the spatial gradient of the elastic modulus of insect cuticle, J. R. Soc. Interface 15 (2018), 20180312, https://doi.org/10.1098/rsif.2018.0312.

[31] D.E. Azofeifa, M. Hernández-Jiménez, E. Libby, A. Solís, C. Barboza-Aguilar, W.E. Vargas, A quantitative assessment approach of feasible optical mechanisms contributing to structural color of golden-like Chrysina aurigans scarab beetles, J. Quant. Spectrosc. Radiat. Transf. 160 (2015) 63–74, https://doi.org/10.1016/j.jqsrt.2015.03.014.

[32] M. Hernández-Jiménez, D. Azofeifa, E. Liby, C. Aguilar, A. Solis, L. Marenco, I. García-Aguilar, A. Hernández, W. Vargas, Qualitative correlation between structural chirality through the cuticle of Chrysina aurigans scarabs and left-handed circular polarization of the reflected light, Opt. Mater. Express 4 (2014) 2632–2645, https://doi.org/10.1364/OME.4.002632.

[33] T.D. Schultz, N.F. Hadley, Structural colors of tiger beetles and their role in heat transfer through the integument, Physiol. Zool. 60 (1987) 737–745, https://doi.org/10.1086/physzool.60.6.30159990.

[34] C. Campos-Fernández, D.E. Azofeifa, M. Hernández-Jiménez, A. Ruiz-Ruiz, W.E. Vargas, Visible light reflection spectra from cuticle layered materials, Opt. Mater. Express 1 (2011) 85, https://doi.org/10.1364/OME.1.000085.

[35] A.C. Neville, Metallic gold and silver colours in some insect cuticles, J. Insect Physiol. 23 (1977) 1267–1274, https://doi.org/10.1016/0022-1910(77)90069-5.

[36] W.C. Aw, F.E. Dowell, J.W.O. Ballard, Using near-infrared spectroscopy to resolve the species, gender, age, and the presence of wolbachia infection in laboratory-reared Drosophila, G3 Genes Genomes Genet. 2 (2012) 1057–1065, https://doi.org/10.1534/g3.112.003103.

[37] F.E. Dowell, J.E. Throne, D. Wang, J.E. Baker, Identifying stored-grain insects using near-infrared spectroscopy, J. Econ. Entomol. 92 (1999) 165–169, https://doi.org/10.1093/jee/92.1.165.

[38] C. Nansen, L.P. Ribeiro, I. Dadour, J.D. Roberts, Detection of temporal changes in insect body reflectance in response to killing agents, PLoS One 10 (2015), e0124866, https://doi.org/10.1371/journal.pone.0124866.

[39] Y. Li, M. Agarwal, Y. Cao, Y. Ren, Effect of synthetic amorphous silica powder on the cuticle of Tribolium castaneum and Sitophilus oryzae using hyperspectral imaging technique, Pest Manag. Sci. 76 (2020) 314–323, https://doi.org/10.1002/ps.5517.

[40] A. Jullien, M. Neradovskiy, A. Scarangella, M. Mitov, Biomimicry of iridescent, patterned insect cuticles: comparison of biological and synthetic, cholesteric microcells using hyperspectral imaging, J. R. Soc. Interface 17 (2020), 20200239, https://doi.org/10.1098/rsif.2020.0239.

[41] Y. Wang, C. Nansen, Y. Zhang, Integrative insect taxonomy based on morphology, mitochondrial DNA, and hyperspectral reflectance profiling: integrative Insect Taxonomy of *Bundera*, Zool. J. Linn. Soc. 177 (2016) 378–394, https://doi.org/10.1111/zoj.12367.

[42] S.C. Voss, P. Magni, I. Dadour, C. Nansen, Reflectance-based determination of age and species of blowfly puparia, Int. J. Leg. Med. 131 (2017) 263–274, https://doi.org/10.1007/s00414-016-1458-5.

[43] M. Harvey, N. Gasz, S. Voss, Entomology-based methods for estimation of postmortem interval, Res. Rep. Forensic Med. Sci. 1 (2016), https://doi.org/10.2147/RRFMS.S68867.

[44] X. Cao, Y. Liu, R. Yu, D. Han, B. Su, A comparison of UAV RGB and multispectral imaging in phenotyping for stay green of wheat population, Rem. Sens. 13 (2021) 5173, https://doi.org/10.3390/rs13245173.

[45] M. Taghizadeh, A.A. Gowen, C.P. O'Donnell, Comparison of hyperspectral imaging with conventional RGB imaging for quality evaluation of Agaricus bisporus mushrooms, Biosyst. Eng. 108 (2011) 191–194, https://doi.org/10.1016/j.biosystemseng.2010.10.005.

[46] C. Garrido-Novell, D. Pérez-Marin, J.M. Amigo, J. Fernández-Novales, J.E. Guerrero, A. Garrido-Varo, Grading and color evolution of apples using RGB and hyperspectral imaging vision cameras, J. Food Eng. 113 (2012) 281–288, https://doi.org/10.1016/j.jfoodeng.2012.05.038.

[47] N. Parisot, C. Vargas-Chávez, C. Goubert, P. Baa-Puyoulet, S. Balmand, L. Beranger, C. Blanc, A. Bonnamour, M. Boulesteix, N. Burlet, F. Calevro, P. Callaerts, T. Chancy, H. Charles, S. Colella, A. Da Silva Barbosa, E. Dell'Aglio, A. Di Genova, G. Febvay, T. Gabaldón, M. Galvão Ferrarini, A. Gerber, B. Gillet, R. Hubley, S. Hughes, E. Jacquin-Joly, J. Maire, M. Marcet-Houben, F. Masson, C. Meslin, N. Montagné, A. Moya, A.T. Ribeiro de Vasconcelos, G. Richard, J. Rosen, M.-F. Sagot, A.F.A. Smit, J.M. Storer, C. Vincent-Monegat, A. Vallier, A. Vigneron, A. Zaidman-Rémy, W. Zamoum, C. Vieira, R. Rebollo, A. Latorre, A. Heddi, The transposable element-rich genome of the cereal pest Sitophilus oryzae, BMC Biol. 19 (2021) 241, https://doi.org/10.1186/s12915-021-01158-2.

[48] A. Heddi, A.-M. Grenier, C. Khatchadourian, H. Charles, P. Nardon, Four intracellular genomes direct weevil biology: nuclear, mitochondrial, principal endosymbiont, and Wolbachia, Proc. Natl. Acad. Sci. USA 96 (1999) 6814–6819, https://doi.org/10.1073/pnas.96.12.6814.

[49] V. Lacotte, E. Dell Aglio, F. Benzaoui, P. Baa-Puyoulet, Weevil Hyperspectral Images Database, 2022, https://doi.org/10.57745/PNWEWS.

[50] V. Lacotte, S. Peignier, M. Raynal, I. Demeaux, F. Delmotte, P. da Silva, Spatial–spectral analysis of hyperspectral images reveals early detection of downy mildew on grapevine leaves, Int. J. Mol. Sci. 23 (2022), 10012, https://doi.org/10.3390/ijms231710012.

[51] T. Kluyver, B. Ragan-Kelley, F. Pérez, B. Granger, M. Bussonnier, J. Frederic, K. Kelley, J. Hamrick, J. Grout, S. Corlay, P. Ivanov, D. Avila, S. Abdalla, C. Willing, in: F. Loizides, B. Scmidt (Eds.), Jupyter Development Team, Jupyter Notebooks – a Publishing Format for Reproducible Computational Workflows, IOS Press, 2016, pp. 87–90, https://doi.org/10.3233/978-1-61499-649-1-87.
[52] F. Pedregosa, G. Varoquaux, A. Gramfort, V. Michel, B. Thirion, O. Grisel, M. Blondel, P. Prettenhofer, R. Weiss, V. Dubourg, J. Vanderplas, A. Passos, D. Cournapeau, Scikit-learn: machine learning in Python, Mach. Learn. Python. (n.d.) 6.
[53] W. McKinney, Pandas: a Foundational Python Library for Data Analysis and Statistics, (n.d.) 9.
[54] C.R. Harris, K.J. Millman, S.J. van der Walt, R. Gommers, P. Virtanen, D. Cournapeau, E. Wieser, J. Taylor, S. Berg, N.J. Smith, R. Kern, M. Picus, S. Hoyer, M. H. van Kerkwijk, M. Brett, A. Haldane, J.F. del Río, M. Wiebe, P. Peterson, P. Gérard-Marchant, K. Sheppard, T. Reddy, W. Weckesser, H. Abbasi, C. Gohlke, T. E. Oliphant, Array programming with NumPy, Nature 585 (2020) 357–362, https://doi.org/10.1038/s41586-020-2649-2.
[55] J.D. Hunter, Matplotlib: a 2D graphics environment, Comput. Sci. Eng. 9 (2007) 90–95, https://doi.org/10.1109/MCSE.2007.55.
[56] M. Waskom, seaborn: statistical data visualization, J. Open Source Softw. 6 (2021) 3021, https://doi.org/10.21105/joss.03021.
[57] T. Boggs, Spectral python (spy), URL Http.www.Spectralpython.Net, 2014.
[58] S. Wold, K. Esbensen, P. Geladi, Principal component analysis, Chemometr. Intell. Lab. Syst. 2 (1987) 37–52, https://doi.org/10.1016/0169-7439(87)80084-9.
[59] S. Lloyd, Least squares quantization in PCM, IEEE Trans. Inf. Theor. 28 (1982) 129–137.
[60] F.T. Liu, K.M. Ting, Z.-H. Zhou, Isolation forest, in: 2008 Eighth Ieee Int. Conf. Data Min., IEEE, 2008, pp. 413–422.
[61] S. Jacquemoud, S. Ustin, Leaf Optical Properties, Cambridge University Press., 2019, https://doi.org/10.1017/9781108686457 (accessed September 7, 2021).
[62] S. Sankaran, A. Mishra, R. Ehsani, C. Davis, A review of advanced techniques for detecting plant diseases, Comput. Electron. Agric. 72 (2010) 1–13, https://doi.org/10.1016/j.compag.2010.02.007.
[63] C.H. Bock, G.H. Poole, P.E. Parker, T.R. Gottwald, Plant disease severity estimated visually, by digital photography and image analysis, and by hyperspectral imaging, Crit. Rev. Plant Sci. 29 (2010) 59–107, https://doi.org/10.1080/07352681003617285.
[64] U. Žibrat, M. Knapič, G. Urek, Plant pests and disease detection using optical sensors/Daljinsko zaznavanje rastlinskih bolezni in škodljivcev, Folia Biol. Geol. 60 (2020) 41, https://doi.org/10.3986/fbg0057.
[65] B. Lu, P. Dao, J. Liu, Y. He, J. Shang, Recent advances of hyperspectral imaging technology and applications in agriculture, Rem. Sens. 12 (2020) 2659, https://doi.org/10.3390/rs12162659.
[66] A. Gowen, C. Odonnell, P. Cullen, G. Downey, J. Frias, Hyperspectral imaging – an emerging process analytical tool for food quality and safety control, Trends Food Sci. Technol. 18 (2007) 590–598, https://doi.org/10.1016/j.tifs.2007.06.001.
[67] A.-K. Mahlein, E.-C. Oerke, U. Steiner, H.-W. Dehne, Recent advances in sensing plant diseases for precision crop protection, Eur. J. Plant Pathol. 133 (2012) 197–209, https://doi.org/10.1007/s10658-011-9878-z.
[68] A.-K. Mahlein, M.T. Kuska, J. Behmann, G. Polder, A. Walter, Hyperspectral sensors and imaging technologies in phytopathology: state of the art, Annu. Rev. Phytopathol. 56 (2018) 535–558, https://doi.org/10.1146/annurev-phyto-080417-050100.
[69] A. Mahlein, Plant disease detection by imaging sensors – parallels and specific demands for precision agriculture and plant phenotyping, Plant Dis. 100 (2016) 241–254, https://doi.org/10.1094/PDIS-03-15-0340-FE.